Climate Dynamics (2023) 61:1867–1885
https://doi.org/10.1007/s00382-023-06660-7

Southern hemisphere monsoonal system during superinterglacial stages: MIS5e, MIS11c and MIS31

Carlos Diego de Sousa Gurjão[1] · Flávio Justino[1] · Gabrielle Pires[1] · Mônica Senna[2] · Douglas Lindemann[3] · Jackson Rodrigues[4]

Received: 2 May 2022 / Accepted: 31 December 2022 / Published online: 6 January 2023

Abstract
The current study investigates changes in Austral Summer Monsoon based on numerical experiments conducted with the coupled ICTP-CGCM model. The interannual variability and intensity of the monsoonal system have been analyzed from vorticity indices and air-sea interaction in Africa, Australia and South America. We focus on interglacial stages MIS5e (127 ka), MIS11c (409 ka) and MIS31 (1072 ka). Results show orbitally-driven decreased summer precipitation and slightly shifted monsoon onset and demise with respect to present day conditions. Sensitivity experiments indicate that monsoons are forced not only by the dominant effect of insolation, but also by remote teleconnections, such as the equatorial Atlantic and Pacific ocean basins. During those interglacial stages, cooling occurs in the Southern Hemisphere whereas Northern Hemisphere substantially warms. This induces meridional displacement of oceanic subtropical high pressure systems and the equatorial convergence zone. Regionally, these mechanisms contribute to droughts over the Amazon and northeastern Brazil, northern Australia and southern Africa. Monsoonal rainfall shows different responses to precessional forcing, as well as the relationship between the monsoon and Niño 3.4 differs among the interglacial stages. Results also indicate a weaker influence of the equatorial Pacific Ocean on the Austral summer monsoon for the MIS31 interglacial stage as compared to current climate conditions across Africa and Australia. On the other hand, South America monsoon is strongly influenced by Niño 3.4 and tropical Atlantic.

Keywords Climate changes · Sea surface temperature · Interglacials · Marine isotope stages

1 Introduction

Previous studies have demonstrated that the strength of global hydrological cycle increases in a warmer climate (Held and Soden 2006), but additional scrutiny is needed to verify hydroclimatic changes under precessional inter-hemispheric seesaw temperature anomalies, with Boreal warming and Austral cooling, as typical of interglacial stages (Justino et al. 2017; Melles et al. 2012; Braconnot et al. 2008; Lisiecki et al. 2005). Despite the large effort reported in the literature to investigate past climatic features, such as precipitation and temperature during distant interglacial stages, evaluation of the spatio-temporal patterns of Southern Hemisphere (SH) monsoon related to changes in external factors is still needed. The SH monsoon characteristics are more noticeable during the austral summer, in which the inversion of the zonal wind component from east to west are highly correlated to significant increases in precipitation rates (Yim et al. 2014; Geen et al. 2020). The seasonal zonal wind shifts in the lower troposphere is a response to the land-ocean thermal contrast which causes rainy summers and dry winters. Investigation of the SH monsoon system under very different climate conditions are very useful to foresee adaptive measures to cope with future changes in the anthropocene. Past changes in the radiative forcing and decreased net energy input have also been responsible

✉ Carlos Diego de Sousa Gurjão
carlosdiegogurjao@gmail.com

[1] Department of Agricultural Engineering, Federal University of Viçosa, Viçosa/MG, Brazil

[2] Departament of Geo-environmental Analysis, Fluminense Federal University, Niterói/RJ, Brazil

[3] Faculty of Meteorology, Federal University of Pelotas, Pelotas/RS, Brazil

[4] Institute of Education, Fluminense Federal University, Angra dos Reis/RJ, Brazil

for the weakening of SH monsoons in the mid-Holocene (D'Agostino et al. 2020).

Simulations of past climate is an excellent tool to provide information on the impact of external forcing in the SH tropical monsoons. Interglacial climates such as occurred during the Marine Isotope Stages (MIS) MIS5e, MIS11c, and MIS31, at approximately 127 ka, 409 ka and 1072 ka (ka = thousand years ago), are characterized by Northern Hemispheric increases in oceanic and terrestrial temperatures. The MIS5e, also known as the Eemian, experienced sudden changes in atmosphere and ocean dynamics in response to strong insolation in the Northern Hemisphere (NH), but weaker in the SH (Yin and Berger 2012; Berger and Loutre 1991; Siccha et al. 2015; Bard et al. 1990). Additional evidences indicate that the northward migration of the Intertropical Convergence Zone (ITCZ) during the Eemian, favor more intense NH summer monsoon as compared with the present climate (Montoya et al. 2000).

The MIS11c (~ 409 ka) also experienced global increase in temperatures in response to enhanced Boreal insolation. However, during this interglacial, the Asian summer monsoon (ASM), as revealed by data from the Yongxing cave, China, does not differ remarkably from monsoon characteristics in the Late Holocene (Zhao et al. 2019). It should be noted that the intensity of the MIS11c warming, is regionally dependent (Yin and Berger 2012; Oppo et al. 1998; Rousseau et al. 1992), rising questions on how MIS11c warming or slight cooling may have induced changes in local precipitation. The MIS31 (~ 1072 ka) is considered the warmest marine isotope stage interval that contributed to substantial melting of NH polar glaciers compared to the present day (Lisiecki et al. 2005; Melles et al. 2012). Modeling studies have demonstrated that orbitally-driven enhanced seasonality affected the global atmospheric and oceanic circulation, which includes the El Niño-Southern Oscillation (ENSO) magnitude and periodicity (Clement et al. 2001; Timmermann et al. 2007; Justino et al. 2017, 2019). Insofar as monsoonal patterns are concerned, it is found that the Indian monsoon was enhanced but no correlation with the ENSO is identified in the MIS31 climate, in contrast with present-day conditions (Trenberth 2011; Yim et al. 2014). In addition, the MIS31 climate shows weak correlation between the equatorial Pacific SST and precipitation indices for Asia, Australia, and Western North Pacific monsoons during this interglacial period (Justino et al. 2017).

Thus, past interglacial temperature contrasts between land and oceanic regions, and the out-of-phase SST pattern induced by the precessional cycle, between both hemispheres might have triggered important changes in seasonal precipitation. Intercomparison among SH monsoon is evaluated based on a series of coupled climate model simulations conducted for different interglacial stages, including all forcing factors such as changes in orbital parameters and greenhouse gases characteristics. The study describes in Sect. 2 the coupled model specifications and experimental modelling setup. Section 3 focuses on results under different perspectives: (1) the control climate is compared to ERA5, (2) changes in the radiative components and temperature are analyzed; and (3) the impact of those changes on atmospheric dynamics responsible for anomalous magnitude, onset and demise of monsoonal precipitation during the interglacials, are shown. Finally, Sect. 4 presents the conclusions in the light of previous investigations and paleo-proxies perspectives.

2 ICTP-CGCM and modeling experimental design

The present study is based on simulations conducted with the Global Coupled Atmosphere-Ocean Circulation Model developed at the International Centre for Theoretical Physics (ICTP-CGCM). The GCM model consists of the global atmospheric climate model "SPEEDY" (version 41) coupled to the Nucleus for European Modeling of the Ocean (NEMO) model (Madec et al. 1998; Madec 2008), and uses the OASIS3 as coupler (Valcke 2013). In computational terms, SPEEDY proofs to be effective in reproducing the main characteristics of the climate system of tropical and extratropical latitudes (Molteni 2003; Kucharski et al. 2006; Justino et al. 2021). The atmospheric component runs at eight vertical levels in T30 horizontal resolution (Kucharski et al. 2016). The oceanic model NEMO runs at 31 vertical levels with thicknesses ranging from 10 to 5000 m of the ocean floor, with 16 levels in the first 200 m. The current version uses a tri-polar ORCA2 configuration with a horizontal grid resolution of 2° and a tropical refinement of 0.5° (Madec 2012).

To investigate the differences between the current climate and the interglacial stages in a systematical way, a series of sensitivity experiments are performed. The first experiment is the control climate (CTRL). It employs an atmospheric CO_2 concentration of 380 ppm and present-day albedo, vegetation, orbital forcing, and topographic boundary conditions as described in Justino et al. (2017, 2019). Three experiments have been carried out for 500 model years to characterize the interglacial intervals. Moreover, the orbital parameters have been set originally according to Berger (1978) and also adopted by Coletti et al. (2015). The atmospheric greenhouse gas concentration is extracted from Bereiter et al. (2015); Lüthi et al. (2008). The study centered the interglacial time at three fixed periods, 127 ka (MIS5e), 409 ka (MIS11c) and 1080 ka (MIS31), however, the orbital forcing is characteristics of the vernal equinox as in the control climate (Table 1). In fact, the position of the vernal Equinox will define when the fall and spring season occur and the length of the season. According to Timm et al.

Table 1 Orbital configurations and greenhouse gases concentrations utilized in the CTRL, MIS5e, MIS11c and MIS31 experiments

Experiment	Date	CO_2 (ppmv)	CH_4 (ppbv)	N_2O (ppbv)	Ecc.	Obl.	Prec.
CTRL	Present	380	801	289	0.01671	23.438	101.37
MIS5e	127 ka BP	287	724	262	0.03938	24.040	272.92
MIS11c	409 ka BP	285	713	285	0.01932	23.781	265.34
MIS31	1.072 ka BP	325	800	288	0.05597	23.898	289.79

(2008) the season varies in length by up to ±6 days. According to their findings, studies on monsoon activity should be compared with fixed angular seasons. For process studies and climate sensitivity investigation the use of fixed angular seasons is imperative. For all experiments the first 400 years of the simulation are not included in the analyses of results. Discussion herein is based on the last 100 years of the 500 years model run.

Several studies have discussed procedure to verify the climatic equilibrium in modeling experiments (Foley 1995; Peltier and Solheim 2004; Otto-Bliesner et al. 2021). In the present case the focus is on atmospheric processes on seasonal timescales, thus, it is reasonable to assume that surface oceanic conditions play the lead role as boundary conditions, with respect to the impact of deep ocean temperatures that vary in much longer timescales (Valdes et al. 2021). It has to be noted that setting up just a fixed time slide do not cover all aspects of the interglacial stages. Notwithstanding, our selected dates are associated with the maxima temperature values throughout those intervals according to Coletti et al. (2015). Verification of the CTRL climate in reproducing present day conditions is based on comparison with the ERA5 reanalysis from 1979 to 2020 (Hersbach 2016). Comparison is conducted for precipitation, zonal wind component (u), sea surface temperatures (SST) and Sea Level Pressure (SLP).

3 Results

3.1 Differences between the CTRL simulation and MIS experiments

3.1.1 CTRL radiative components and temperature

There are no substantial changes of the atmospheric composition among the interglacials (Table 1), but reduced concentrations favour slightly cooling conditions with respect to CTRL, due to lower atmospheric CO_2 concentration and resulted weaker greenhouse capacity of the atmosphere. These features contrast with modifications of the Earth's orbit during the interglacial epochs, in particular the precessional cycle. Figure 1 shows zonally averaged radiative components at the top of atmosphere (TOA) based on ERA5 and the CTRL simulation.

Overall, the coupled model is able to represent the energy balance at the TOA and surface. The ICTP-CGCM underestimates ERA5 values by about 5% at the TOA (Fig. 1a). Good match between ERA5 and the model is found in the zonal distribution, but the presence of the ITCZ in the equatorial region leads to more pronounced differences across 10° S and 10° N. Atmospheric models running under lower resolution show drawbacks in reproducing meso-scale convective system in the tropics leading to modified radiative balance (Tomita et al. 2005; Satoh et al. 2019). In the polar regions and extratropics as expected (Fig. 1a), more energy is emitted to space via longwave (LW) radiation than is provided by the shortwave (SW) component. In general grounds, the modeled radiative budget (Rn) is well represented, that in fact, is responsable for the large-scale atmospheric and oceanic circulations. It should be emphasized that estimates of the radiative balance has been for many years a challenging task associated with improvements of coupled models (Wild 2020).

Differences of short wave radiation at the top of the atmosphere during the MIS5e, MIS11c and MIS31, with respect to the CTRL climate (Fig. 1b–d), show the large influence of modified orbital parameters from June to November in the SH tropics, with an increase of 60 Wm^{-2} in the MIS5e, and 20 Wm^{-2} in MIS11c (Fig. 1b–c). The most significant increase is, however, observed in NH where the shortwave radiation is larger than the CTRL values in summer. The MIS31 is among the interglacial periods the most affected by orbital changes from March to October. From November to March, the SH experiences reduction in the amount of incoming energy, which is the dominant period of the Austral monsoonal system (Fig. 1b–d). This may indicate that the attribution of warmer planetary or hemispheric climate in past interglacials, with respect to today's climate, in particular based on paleoreconstructions analyses, should be taken with care due to enhanced seasonal variability and regional characteristics.

Figure 2 shows that modified orbital parameters and subsequent changes of incident solar radiation, result in anomalous near surface air temperatures. Differences between the interglacials and current climate across the continents are characterized by cooling from November to February (NDJF, Fig. 2a–c–e). This gradually turns to warmer conditions in Boreal spring with largest anomalies in summer, which are reproduced by the annual anomalous pattern

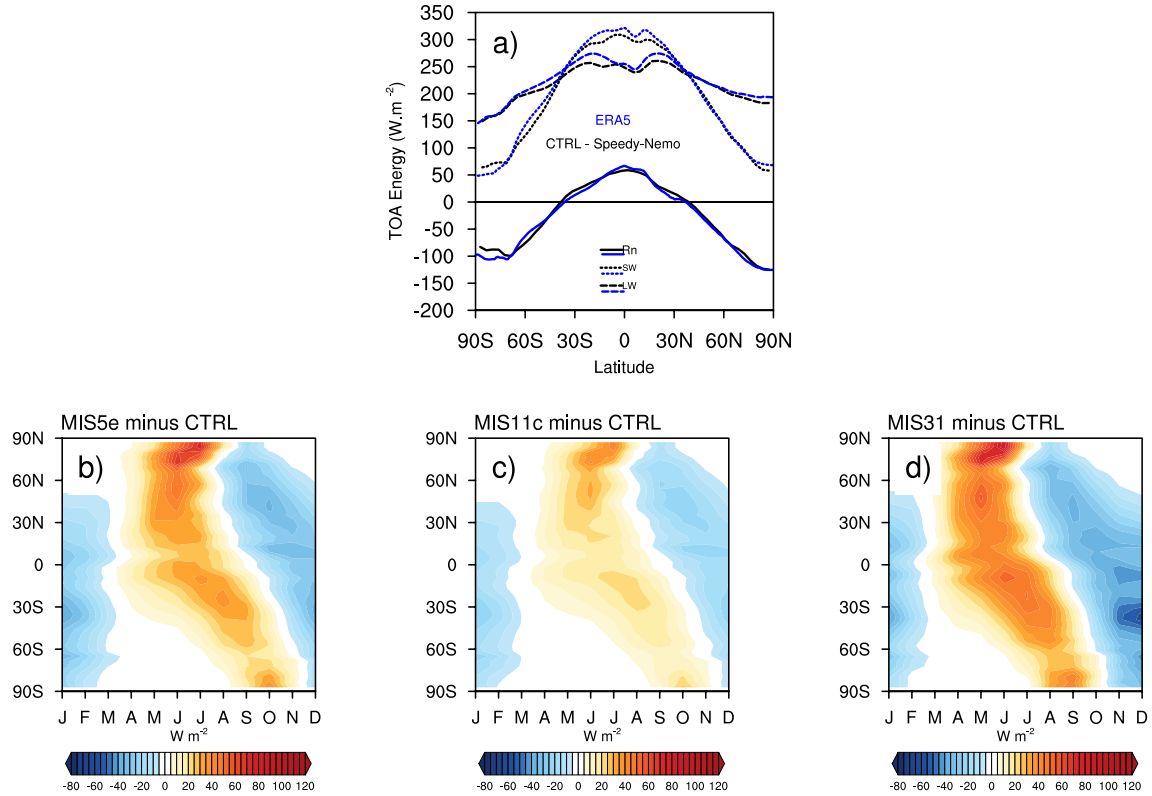

Fig. 1 Zonal mean energy budget components (Wm^{-2}) in the top-of-atmosphere (TOA) (**a**). **b** Shows differences of shortwave radiation at the top of the atmosphere (Wm^{-2}) between MIS-5E minus CTRL, MIS-11C minus CTRL (**c**) and MIS-31 minus CTRL (**d**). Values in (**a**) are based on ERA5 reanalysis and the ICTP-CGCM coupled model

(Fig. 2b–d–f). The SH summer monsoons, which are dominant in NDJF months, can be severely affected by surface thermal changes not only causing a reduction in the amount of rainfall, but also by inducing distinct onset and demise periods. Surface condition are determinant for SH monsoons because soil moisture and evapotranspiration play an important role at early stages of the monsoon (D'Agostino et al. 2020; Collini et al. 2008).

The substantial warming delivered over the continents as shown by annual time averaged temperatures (Fig. 2b–f), induces a northward migration of the ITCZ, as well as a weakening of the southern trade winds (Justino et al. 2019). The modified orbital forcing leads to reduced radiative balance in the Southern Hemisphere (SH) and associated warming across the Northern Hemisphere (NH). This pattern induces an inter-hemispheric thermal gradient that shift northward the ITCZ with respect to its regular position. This is also related to the anomalous pattern of SLP. Indeed, during the interglacials stages the SH (NH) experiences higher (lower) SLP with respect to the CTRL climate. This intensified middle-latitudes high pressure centers, modify the strength of the trade winds, prevailing southwesterly and weakening northeasterly, driving the northward migration of the ITCZ. It is not speculative to argue that these anomalous features will be associated with modifications in the thermal ocean-land characteristics, impacting the monsoonal system.

3.1.2 Annual distribution of precipitation and SH monsoonal characteristics

To identify the SH monsoons spatial domain, the amplitude of the first harmonic of precipitation has been computed (Fig. 3a, b). The first harmonic characterizes regions where the annual cycle is dominant explaining more than 80% of the variance. This fits nicely with monsoonal features. Harmonic analyses also known as Fourier transformation, are computed on a series of sine and cosine functions which may be used to verify differences in the precipitation magnitude between the rainy and dry seasons, for instance.

Figure 3b shows the first harmonic amplitude of precipitation, based on a 100-year CTRL simulation. The ICTP-CGCM is capable to reasonable locate the larger amplitude of precipitation over the South African Monsoon System (SAF), the Australian Monsoon System (AUS) and the South American Monsoon System (SAM) regions (Fig. 3a). The CTRL experiment (Fig. 3b), however, overestimates the 1st harmonic amplitudes by 5 mm/day in particular across

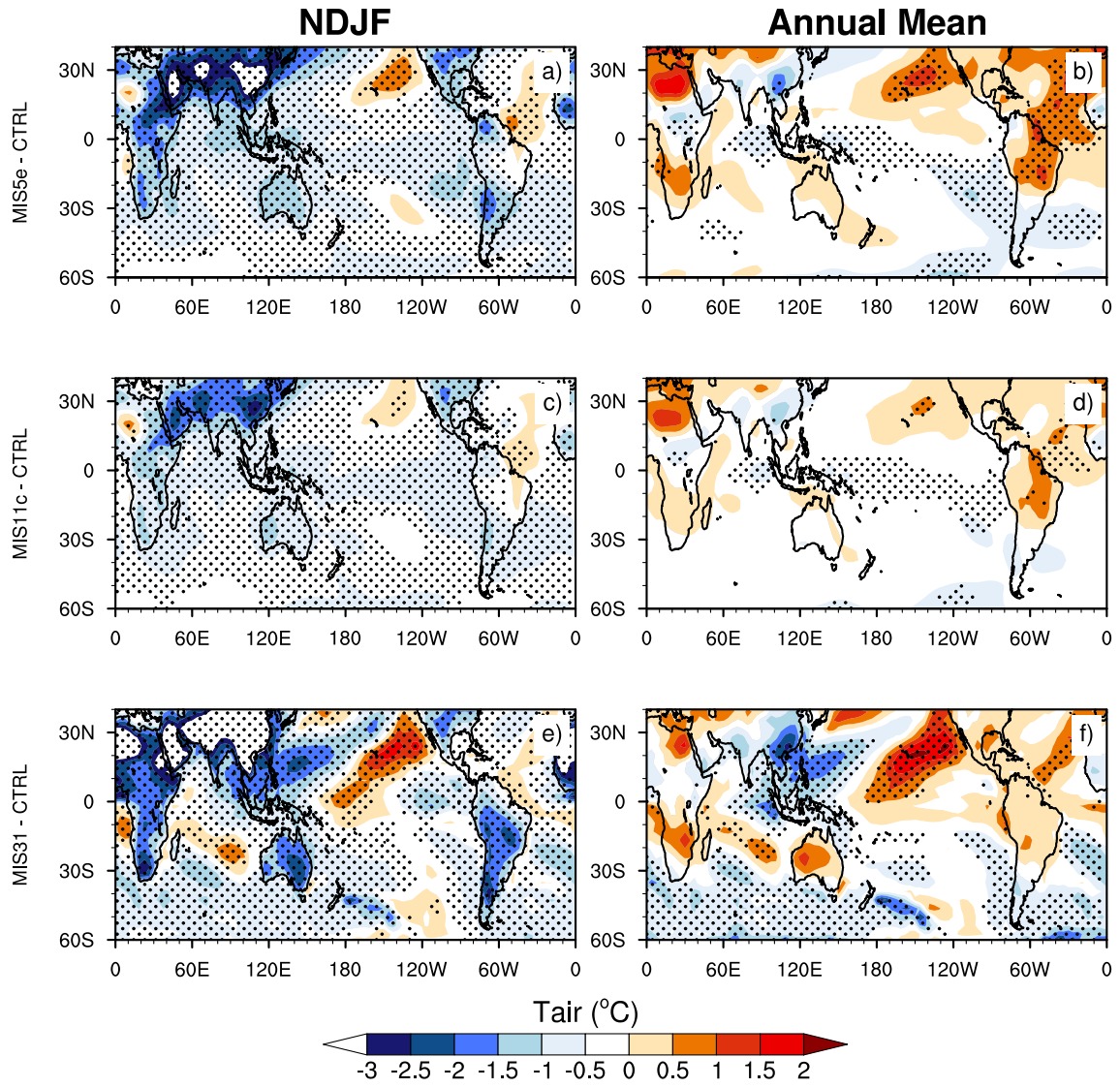

Fig. 2 NDJF mean surface temperature differences (°C) between MIS5e and CTRL (**a**), MIS11c and CTRL (**c**), and MIS31 and CTRL (**e**). (**b**–**d**–**f**) is the same as (**a**–**c**–**e**) but for mean annual differences. Dotted regions are statistically significant at the 95% confidence level

SAMS, in comparison to values delivered by ERA5 dataset (Fig. 3a, b). Drawbacks in simulating tropical dynamics in coupled models, arise due to limitations in reproducing ocean-atmosphere interaction due to their lower resolution, as compared to processes in the extratropics. This occurs becausec onvection, turbulent heat fluxes and diabatic processes are more difficult to be properly simulated (Flato et al. 2014; Neelin et al. 1994; Marengo et al. 2012).

Furthermore, it should be mentioned that the CTRL climate discussed here shows differences from ERA5, in part because time intervals used are not the same. The CTRL is based on a 100 years simulation forced with initial conditions correspondent to 1950. Certainly, these different intervals drive slightly distinct climates, also due to the ICTP-CGCM interannual and interdecadal variability, which may differ with respect to ERA5 conditions computed from 1979 to 2020.

The CTRL climate delivers higher precipitation as reproduced by areal averages over SAMS and AUSMS and lower values are found for SAFMS (Fig. 3). Among the monsoons, higher daily precipitation amount is delivered for the AUSMS (≈ 10 mm/day), whereas lower values are observed in the SAFMS (≈ 6 mm/day). This is highlighted from November to March. Regionally, 70% of annual rainfall occurs during the NDJF months. ERA5 shows along the SAMS, SAFMS and AUSMS domains, magnitudes by about 7, 9 and 8 mm/day (Fig. 3c–e).

Correlation analyses based on monsoon indices as represented by the zonal circulation and the areal averaged rainfall show reasonable correspondence between ERA5

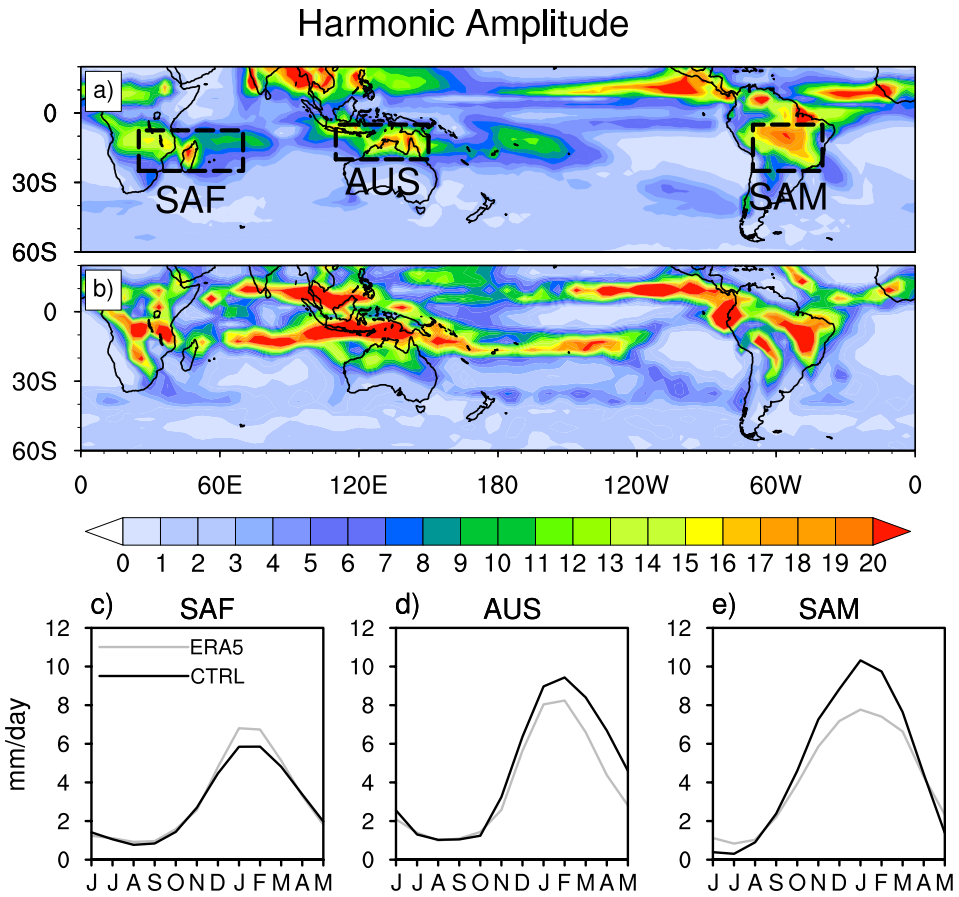

Fig. 3 Amplitude of the 1st harmonic based on ERA5 (**a**), and the CTRL simulation (**b**). **c**, **d** and **e** show the climatological annual cycle of areal averaged precipitation across the SAFSM, AUSSM and SASM domains (mm/day)

Table 2 Correlation coefficients between the regional monsoon precipitation in the rectangular domains and respective vorticity indices

	Monsoon domain	Monsoon (index)	ERA5 CC	CTRL CC	MIS5e CC	MIS11c CC	MIS31 CC
SAFSM	(0–20° S, 10° E–50° E)	U_{850}(5° S–15° S, 20° E–50° E)–U_{850}(20° S–30° S, 30° E–55° E)	**0.52**	**0.74**	**0.76**	**0.78**	**0.77**
AUSSM	(0–20° S, 105° E–160° E)	U_{850}(0–15° S, 90° E–130° E)–U_{850}(20° S–30° S, 100° E–140° E)	**0.93**	**0.86**	**0.72**	**0.74**	**0.73**
SASM	(5° S–25° S, 70° W–40° W)	U_{850}(5° S–20° S, 90° E–130° E)–U_{850}(20° S–30° S, 100° E–140° E)	**0.80**	**0.37**	**0.50**	**0.65**	**0.31**

Bold values indicate statistical significance at the 95% level

and the CTRL run (Table 2). Values up to 0.86 and 0.74 are found for AUSMS and SAFMS, but much lower correlation is delivered for SAMS (0.37). This indicates that insofar as the SAMS is concerned, the vorticity index in the CTRL run does not match the precipitation temporal characteristics related to the monsoon. The presence of the Andes, the recurrent cold fronts and the Amazonian contribution to the SAMS through evapotranspiration, are complex features that may weak the correlation between the vorticity index and SAMS precipitation in the ICTP-CGCM. It may be argue that nearby oceanic processes exert an important role to define the SAM. These processes involve SST changes in the southwestern Atlantic Ocean, which impact in two-ways interaction the strength of the South Atlantic Convergence Zone (SACZ), by modifying the maritime water vapor transport as well as the heat flux onto continental regions (Pezzi et al. 2022; Jorgetti et al. 2014). The SST and oceanic conditions impact on the monsoonal system are discussed in more detail in the following sections.

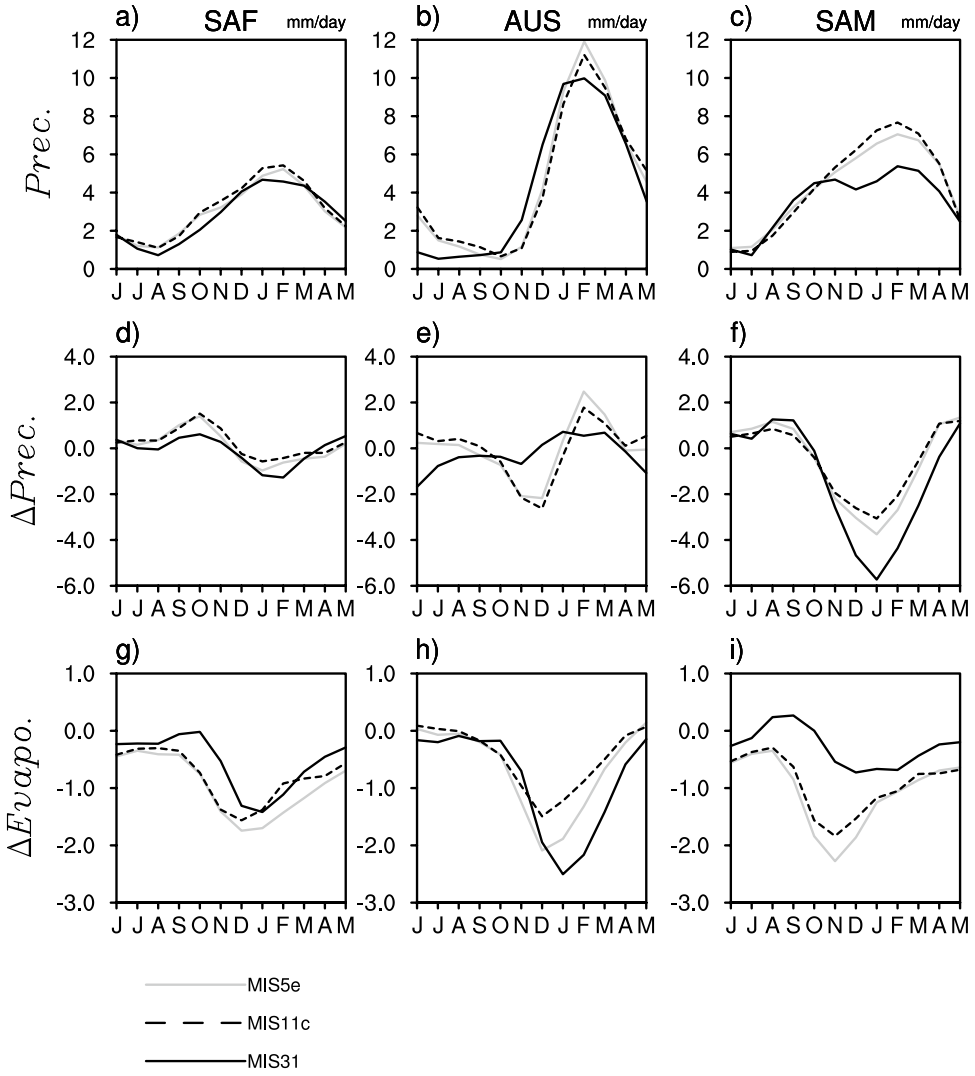

Fig. 4 Climatological annual cycle of precipitation for SAF (**a**), AUS (**b**), and SAM (**c**). **d**–**f** show differences of precipitation (*ΔPrec*) between the MIS5e, MIS11c, and MIS31 with respect to CTRL conditions. **g**–**i** are the same as **d**–**f** but for evapotranspiration (mm/day, *ΔEvapo*.)

3.1.3 Monsoonal precipitation

Changes in insolation during the interglacials lead to drastically modified monsoonal precipitation amounts (Fig. 4). With respect to CTRL, results show that increased precipitation occurs in the dry season (June, July and August) in particular for SAFMS and SAMS (Fig. 4a, c). These features are enhanced in the MIS11c and MIS5e, and may represent a slightly shift in the rainy period over the two monsoons domains. In AUSMS, larger changes are depicted from October to February, with a drop in rainfall (Fig. 4e), therefrom an increase of the rainfall is found until April. The MIS31 delivers remarkable changes of precipitation, with drier conditions in the SAMS, with precipitation as low as 60% in comparison to CTRL (Fig. 4f). Reduction is also found for the other SH systems, the weakening of the SAFMS precipitation occurs during the summer months, whereas for the AUSMS drier conditions are found from June to December (Fig. 4d, e).

Changes in surface conditions such as shown by evapotranspiration (ET, Fig. 4g–i), in line with those depicted by precipitation in the SAFMS, indicate the importance of surface processes and precipitation, in particular soil moisture. Analyses for the other two SH monsoon do not demonstrate a close relationship between ET and precipitation. However, reduced precipitation over the SH monsoon regions, in turn, also leads to less water available for evapotranspiration. In the AUSMS, enhanced monsoon rainfall is accompanied by reduced ET, which lead to assume that the AUSMS during these interglacial, experiences large contribution from water vapor transport originating from outside the monsoonal domain.

The SAMS pattern shows a time lag relationship, in which the reduction of ET leads by two months negative anomalies of precipitation in the MIS11c and MIS5e. The

delay in the rainy season can be triggered mainly by the low rates of evapotranspiration in the Amazon and Cerrado by the end of the dry season. The seasonal rainfall reduction related to evapotranspiration, is also forced by the weakening mechanism of the SAMS. In the case of MIS31, changes in ET influence in lower degree modification of precipitation, with respect to the other interglacials (Fig. 4g–i).

Changes in surface conditions such as shown by evapotranspiration (ET, Fig. 4g–i) are in line with those depicted by precipitation in the SAFMS, indicating the importance of interaction between surface processes and precipitation, in particular soil moisture. Analyses for the other two SH monsoon do not demonstrate a close relationship between ET and precipitation. However, reduced precipitation leads to lower soil moisture and reduced evapotranspiration. In the AUSMS, enhanced monsoonal rainfall is accompanied by reduced ET, which may indicate that the AUSMS during these interglacial, experiences large contribution from water vapor transport originating from outside regions of the monsoonal domain. The pattern over the SAMS shows a time lag relationship, in which lowest ET leads by two months negative anomalies of precipitation in the MIS11c and MIS5e. The delay in the rainy season can be triggered mainly by low rates of evapotranspiration in the Amazon and Cerrado, at the end of the dry season. In the case of MIS31, changes in ET are not closely related to precipitation, with respect to the other interglacials (Fig. 4g–i).

The onset and demise of the rainy season related to monsoonal characteristics is also evaluated by the Hovmöller diagram (Fig. 5), which shows the inversion of the zonal wind; eastward winds in the dry season and westward winds for the rainy season. In general, changes in atmospheric circulation via the inversion of the zonal wind are well simulated by the ICTP-CGCM (Fig. 5a–c).

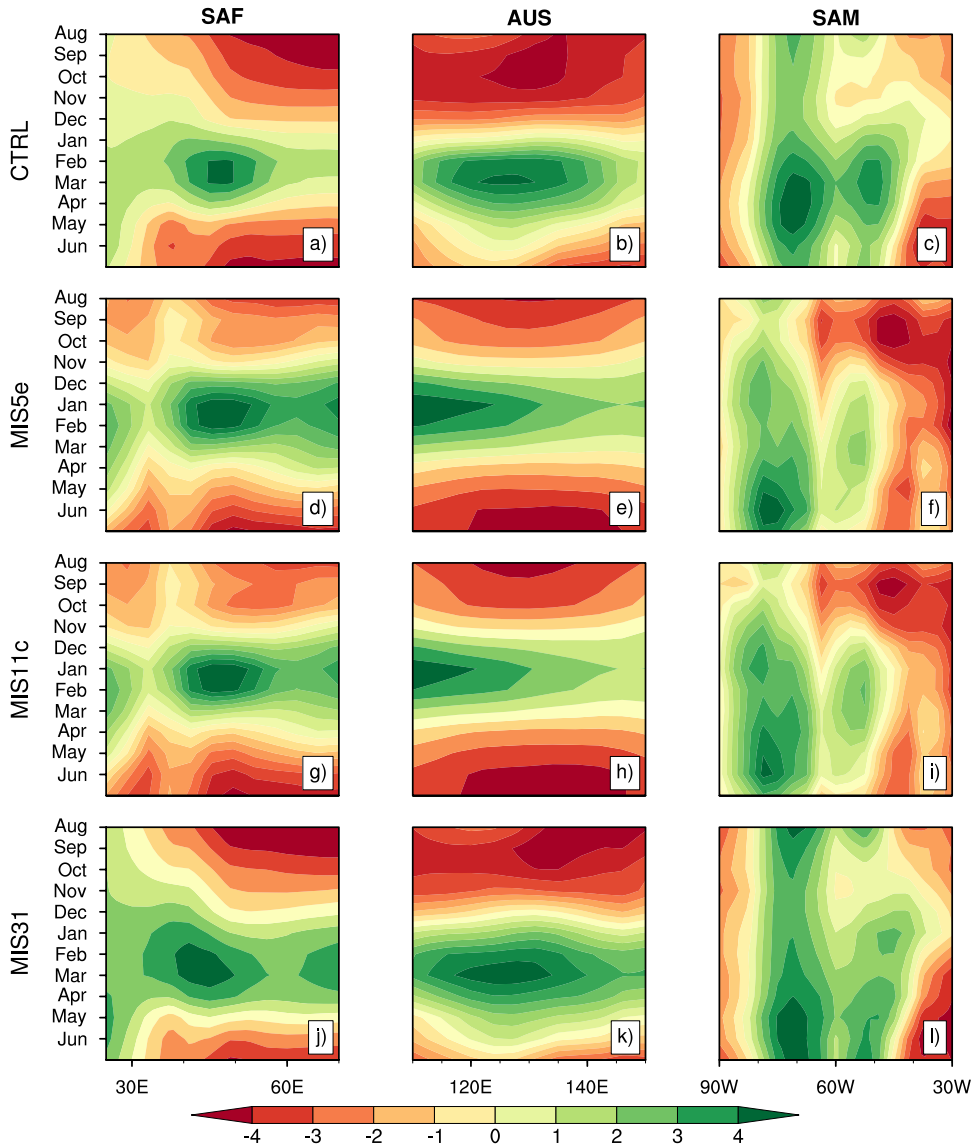

Fig. 5 Longitude-time cross-section of climatological zonal wind (m/s) at 850 hPa averaged between latitudes 7.5° S–25° S (SAF), 5° S–20° S (AUS) and 5° S–25° S (SAM). Westerlies are lime-green (positive) and easterlies are yellow-red (negative)

Similar pattern is depicted for the SAFMS and AUSMS by indicating an east-west wind shift during the summer months (Fig. 5a, b). However, different pattern emerges for the SAMS where wind transition is not clearly seen. In the SAMS wind features are longitudinal and confined to the eastbound of the monsoon between 60°–30° W(Fig. 5c). Despite reasonably reproducing the monsoon annual cycle, the ICTP-CGCM does not relate the wind features to precipitation in the SAMS domain. This is associated with the topographic barrier imposed by the Andes, which channels throughout the year the easterly Atlantic flow, hampering the seasonal shift, as discussed by Nogués-Paegle et al. (2002).

The MIS5e and MIS11c deliver a semi-annual component that is most evident in the SAFMS and AUSMS but is absent in the MIS31, which exhibits a well defined annual cycle (Fig. 5j, k). Indeed, stronger annual cycle in the MIS31 has been found by Justino et al. (2019). Weaker interannual ENSO may act in line to enhance the orbital forcing (Carré et al. 2021). The SAMS is different because it experiences large changes related to the implementation of the orbital forcing (Fig. 5f, i, j). For this monsoon, the MIS5e

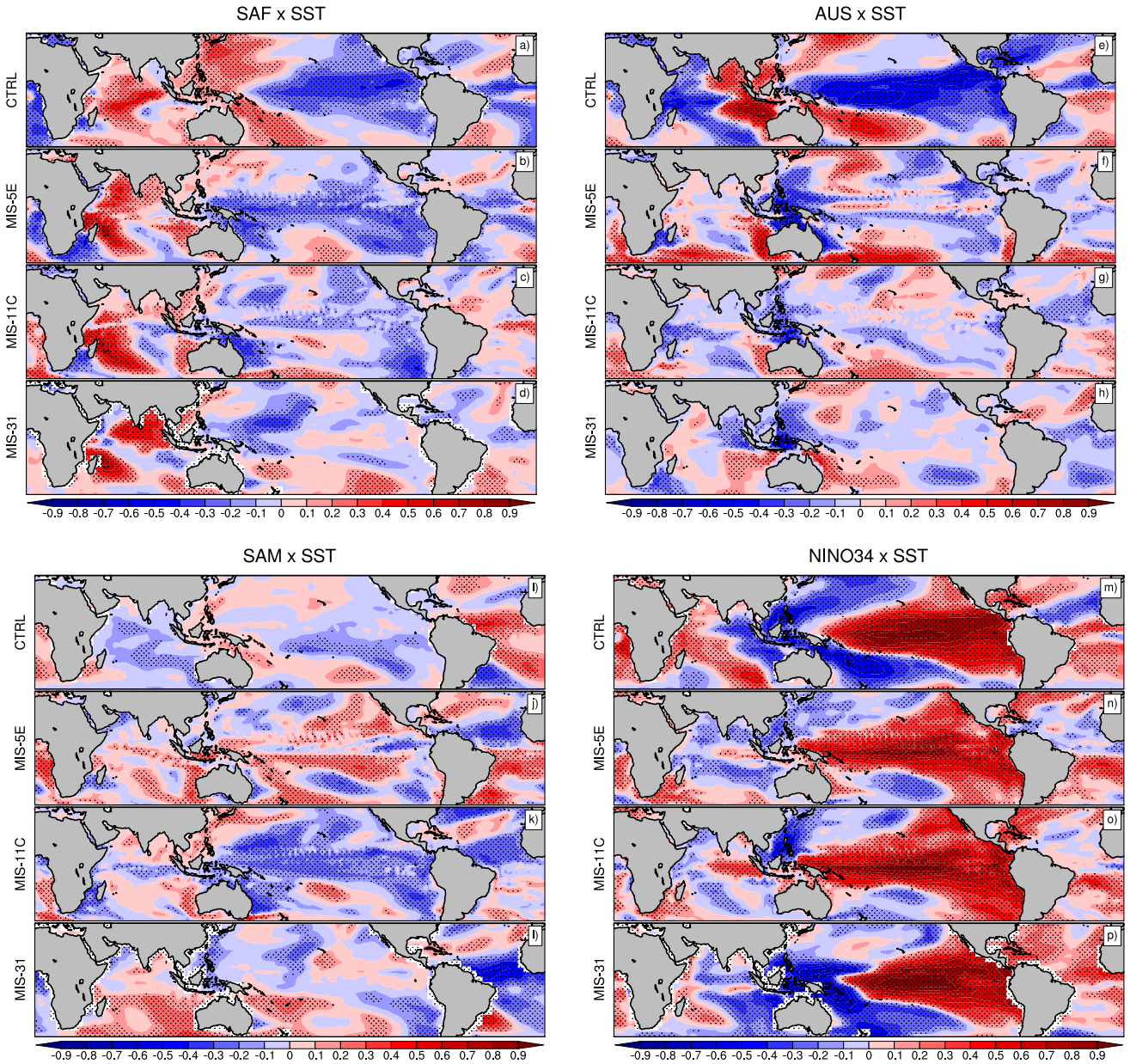

Fig. 6 Correlation coefficient between regional summer monsoons precipitation indices and SST for SAF (**a**–**d**), AUS (**e**–**h**) and SAM (**i**–**l**). **m**–**p** display the correlation between the ENSO and SST anomalies. Also shown is the 95% significant areas (dotted grids)

and 11c differ substantially from the CRTL with increased zonal wind shear, and subsequently increased convergence over 45° W, from December to March (Fig. 5j, i). Moreover, it is found drastically modified circulation from August to November with respect to CTRL. Strong westerly flow is evident in the MIS5e and MIS11c climates from 60–30° W, which results from intensified sub-tropical Atlantic high.

In order to evaluate in more detail mechanisms responsible for interglacial monsoonal changes, it is shown in Fig. 6, the correlation pattern between the SAFMS, AUSMS and SAMS vorticity indices and SST changes. It highlights that similarities between the SAFMS and AUSMS under CTRL conditions, do not propagate through interglacials stages (Fig. 6a–h). The MIS5e exhibits a pattern, in particular across the Pacific Ocean, that is between CTRL and the MIS11c and MIS31. For instances, both monsoon seem to be well correlated with Pacific and Indian Ocean SST in the CTRL climate, however, in MIS11c and MIS31, the SAFMS is highly related to Indian Ocean only (Fig. 6c, d). In the AUSMS case, changes over the warm pool Pacific region are dominant insofar as SST are concerned because weak correlation are found over the eastern Equatorial Pacific region (Fig. 6g, h).

As demonstrated by previous discussion, the SAMS (Fig. 6i–l) differs substantially from other monsoons. The Atlantic Ocean exerts an important role which is dependent upon the interglacial investigated. Indeed, under CTRL conditions higher positive correlations are found between precipitation and warmer Atlantic SST, under La Niña-like background (Fig. 6i). Turning to MIS5e, the presence of the Tropical Atlantic variability (TAV, (Cabos et al. 2019) is enhanced with respect to CTRL, with a well defined dipole (Fig. 6j). The SST correlation pattern may indicate a southward position of the ITCZ, due to northern Atlantic cooling, but it has also to be noted that other forcing such as the meridional pressure gradient infleunces the ITCZ position. Positive correlation also in the southwestern Atlantic is other feature that indicates intensification of the South Atlantic Convergence Zone (SACZ). The relationship between SST and SAMS precipitation for the MIS11c and MIS31 demonstrated that the positive correlation is weaker in the southern Atlantic in the MIS11c, whereas an overall anticorrelation is found in the MIS31 (Fig. 6l). In general, the MIS31 exhibits contrasting values with respect to the CTRL (Fig. 6i, l), insofar as the SAM is concerned.

The eastern tropical Pacific exhibits a strong relationship with continental rainfall, particularly due to ENSO characteristics. ENSO events have been defined based on Empirical Orthogonal Function (EOF) of monthly SST anomalies over the tropical Pacific. El Niño and La Niña are the first principal component (PC) time series over the equatorial Pacific domain (20 N–20 S). Table 3 indicates that during El Niño events, monsoonal precipitation of the three analyzed sectors is reduced with larger changes for AUSM in both ERA5 and in CTRL. These significant correlations, also reveal that ENSO can drive interannual variability over the summer monsoons for the MIS5e and MIS11c, with exception of the AUSSM sector. On the other hand, the AUSSM is negatively correlated with ENSO in MIS31 at a 95% confidence level. Although, the spatio-temporal variability patterns of rainfall are different for each interglacial, it depends on the intensity of individual ENSO events. The correlations between SH continental monsoon rainfall and TAV shows that under CTRL conditions most correlations are not significant. Turning to the interglacial intervals, the analyses demonstrate weaker correlations with respect to ENSO, but significant over the SAMS in the MIS5e. Interesting is that correlations between TAV and SAMS (− 0.33) are higher than correlations based on ENSO (− 0.29) (Table 3).

3.1.4 Spatial patterns of Precipitation and SLP

Figures 7 and 8 show differences in precipitation and SLP (interglacial minus control) overlaid with significant correlation (dotted), between the regional monsoon vorticity index; and precipitation and SLP. Analyses of SLP can be further used to determine convergence and divergent flows which may increase or suppress precipitation.

During the DJFM there is a reduction in rainfall in southern/southeast Africa and much of South America for MIS5e and MIS11c, with values between − 2 and − 5 mm/day (7a–f, with respect to CTRL. Precipitation increases are found in the Indonesian Archipelago and southern Australia by up to 4 mm/day (Fig. 7b–e). The dominant effect

Table 3 Correlation coefficients between ENSO, TAV indices and the regional monsoon precipitation

Austral Summer (DJFM)	ERA5		CTRL		MIS5e		MIS11c		MIS31	
Index	ENSO	TAV	ENSO	TAV	ENSO	TAV	ENSO	TAV	ENSO	TAV
Monsoon domain										
SAFSM	**− 0.40**	− 0.25	**− 0.36**	**0.26**	**− 0.33**	0.14	**− 0.27**	0.1	− 0.14	0.13
AUSSM	**− 0.70**	0.26	**− 0.56**	0.16	− 0.05	0.01	− 0.04	− 0.14	**−0.30**	0.04
SASM	**− 0.30**	**0.30**	**− 0.20**	0.18	**− 0.29**	**− 0.33**	**− 0.23**	− 0.11	− 0.03	− 0.15

Bold values indicate statistical significance at the 95% level

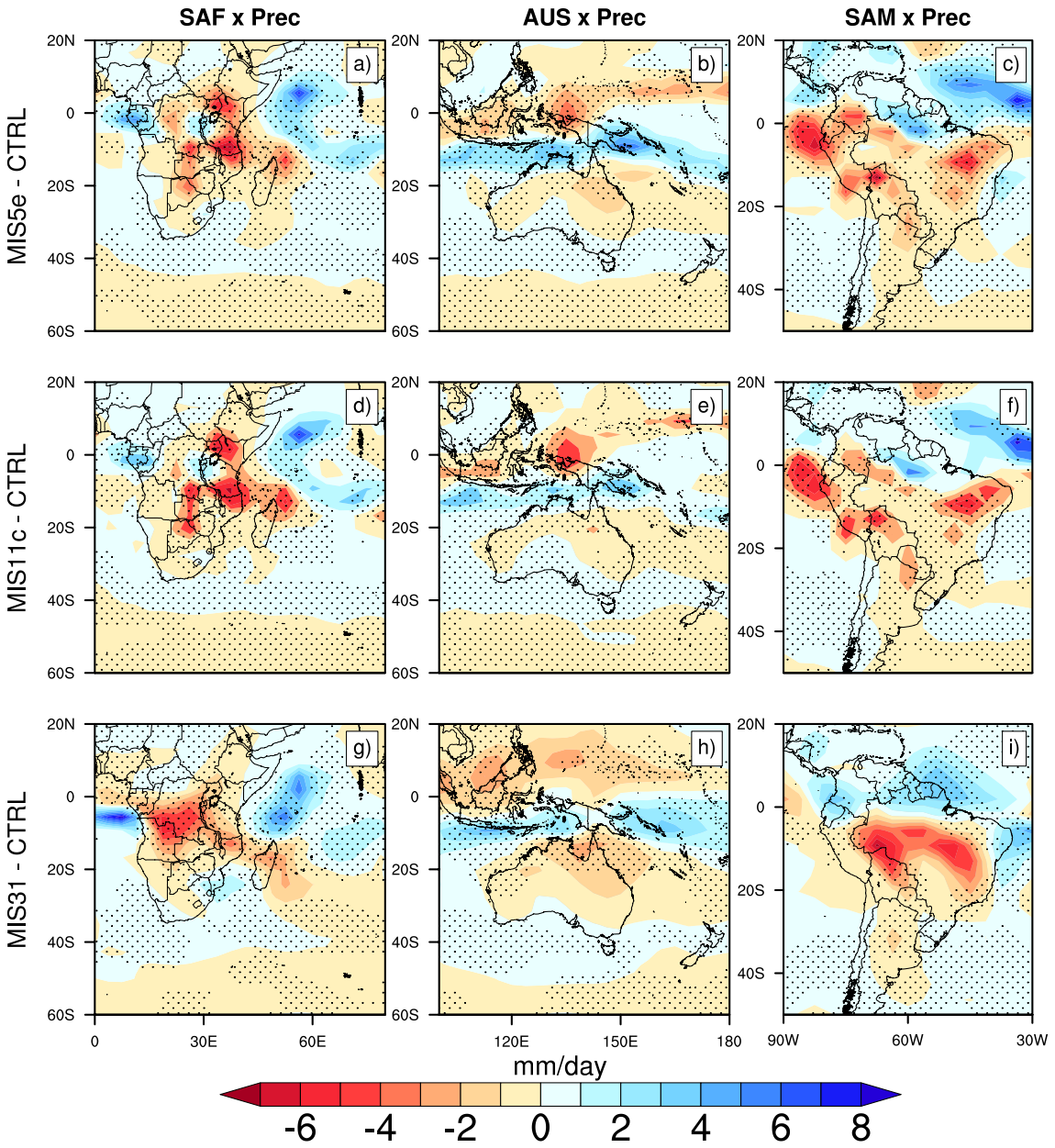

Fig. 7 Austral monsoon precipitation anomalies between MIS5e minus CTRL (**a**–**c**); MIS11c minus CTRL (**d**–**f**) and MIS31 minus CTRL (**g**–**i**). Dots indicate significant correlation between the regional monsoonal vorticity index and precipitation

of the orbital forcing in all 3 interglacials is highlighted as reduced precipitation across most of continental regions. In the MIS31, reduced rainfall in Africa and South America show values between − 2 and − 6 mm/day (Fig. 7g–i). Rainfall increases in northern Amazon and semiarid Northeast Brazil (3 mm/day), but there is no evidence that this is linked to monsoonal changes. It should be noted that precipitation in Australia are less affected by the implementation of the orbital forcing. Most anomalies range between ± 2 mm/day, and are not statistically significant in MIS31.

Analyses of differences of SLP may clarify causes of precipitation changes. The SLP anomalies between the interglacials experiments (MIS5e, MIS11c e MIS31) and CTRL, exhibit statistically significant increased pressure in line with precipitation reduction over SAFMS, AUSMS and SAMS regions (Fig. 8). Differences of MIS11c and CTRL show slight reduction in SLP across southern Australia and south-central Brazil (Fig. 8e, f). Those low pressure anomalies induce precipitation (Fig. 7e) in Australia by enhancing convection and upward motion. It has to be noticed that this drop in SLP during the MIS11c

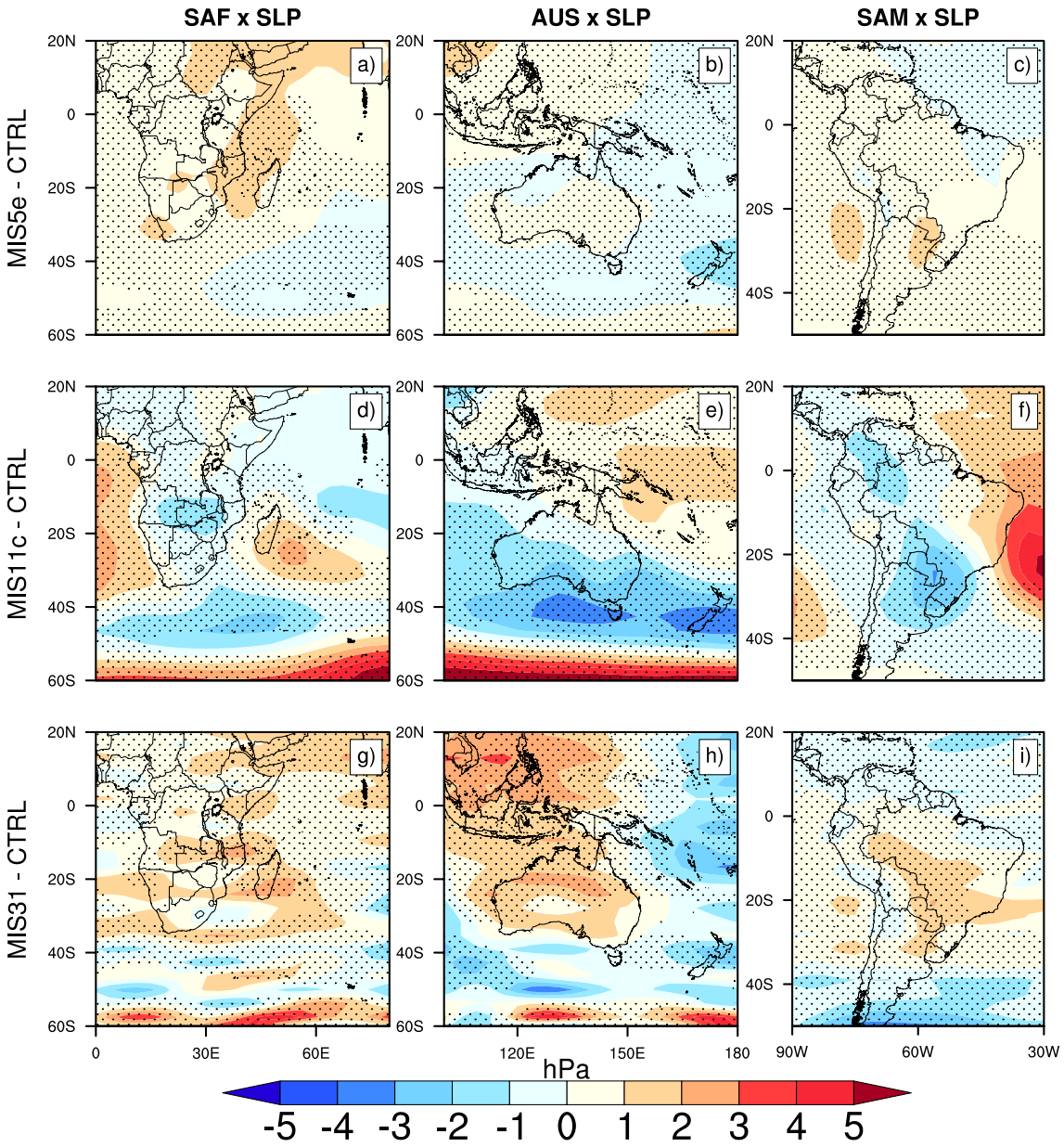

Fig. 8 Same as Fig. 7 but for SLP

in southern Brazil/South America, theoretically would increase the frequency of subtropical frontal systems, passing onto the SAMS region, but the high pressure anomaly associated with the subtropical Atlantic high, leads to a blocking situation hampering the subtropical system to move northwards. Thus, leading to dryness in most of Brazil during the interglacial. In the MIS31, most striking feature is related to cooling in western Pacific by up to − 3 °C, in particular over the AUSMS domain. This results in positive SLP anomalies characteristics of permanent El Niño conditions (Figs. 2f and 8h), reduced AUSMS monsoonal precipitation (Fig. 7h).

3.1.5 Intercomparison between modeled precipitation and proxy data

Paleoclimate simulations are able to simulate Earth's past climate, but comparison with reconstruction are still necessary to reveal model-proxies differences, in regions where models may struggle to represent particular atmospheric/oceanic features. Thus, indicating climate mechanisms that should be addressed in more detail (Braconnot et al. 2012). Justino et al. (2017) provides an evaluation of modeled MIS31 surface temperature and proxies, in which demonstrated that the ICTP-CGCM is able to reproduce

reconstructions, differing only by ± 1 °C, but larger values up to 3 °C are found in the extratropics. These large differences have been attributed to reduced NH sea-ice cover, and therefore higher SSTs.

The three interglacials are warmer (colder) in the NH (SH) than the CTRL climate (Table 4). It is also worth mentioning that the ICTP-CGCM model simulates lower temperatures than the reconstructions primarily in the Austral extratropical region for the MIS5e and MIS11c. These two interglacials show warmer temperatures in the NH (2–6 °C). The paleoproxies also exhibits caveats because in some cases it may reproduce long term changes that are dictated by a particular seasonal strength, such as demonstrated by Liu et al. (2014). This argumentation is not used to justify differences between model and reconstructions, but usefully serves to indicate that reconstructions represent local conditions that can be smoother in a grid box representation.

Hydroclimatic reconstructions from MIS5e and MIS11c are shown in Table 5 and Fig. 9, across the 5° N–33° S domain. This allows to identify the precipitation and evaporation relationship, and therefore atmospheric humidity in both time slices, with respect to CTRL climate. By evaluating proxies for individual latitudinal bands shows that between 5° N–5° S, drier conditions prevailed during NDJF months in the MIS5e, with exception of African sites in reconstruction and model results (red circles in Fig. 9). These conditions are present not only during the monsoonal season bit it is distributed throughout the year (Fig. 9a–c).

From 6° S to 15° S most reconstructions are marked by increased humidity (blue circles in Fig. 9), differing from simulated values, that during the monsoonal season show dryer conditions, in particular in central Africa and Australia. Agreement is found over Indonesian Archipelago, east Africa and the Andes. By comparing reconstructions and

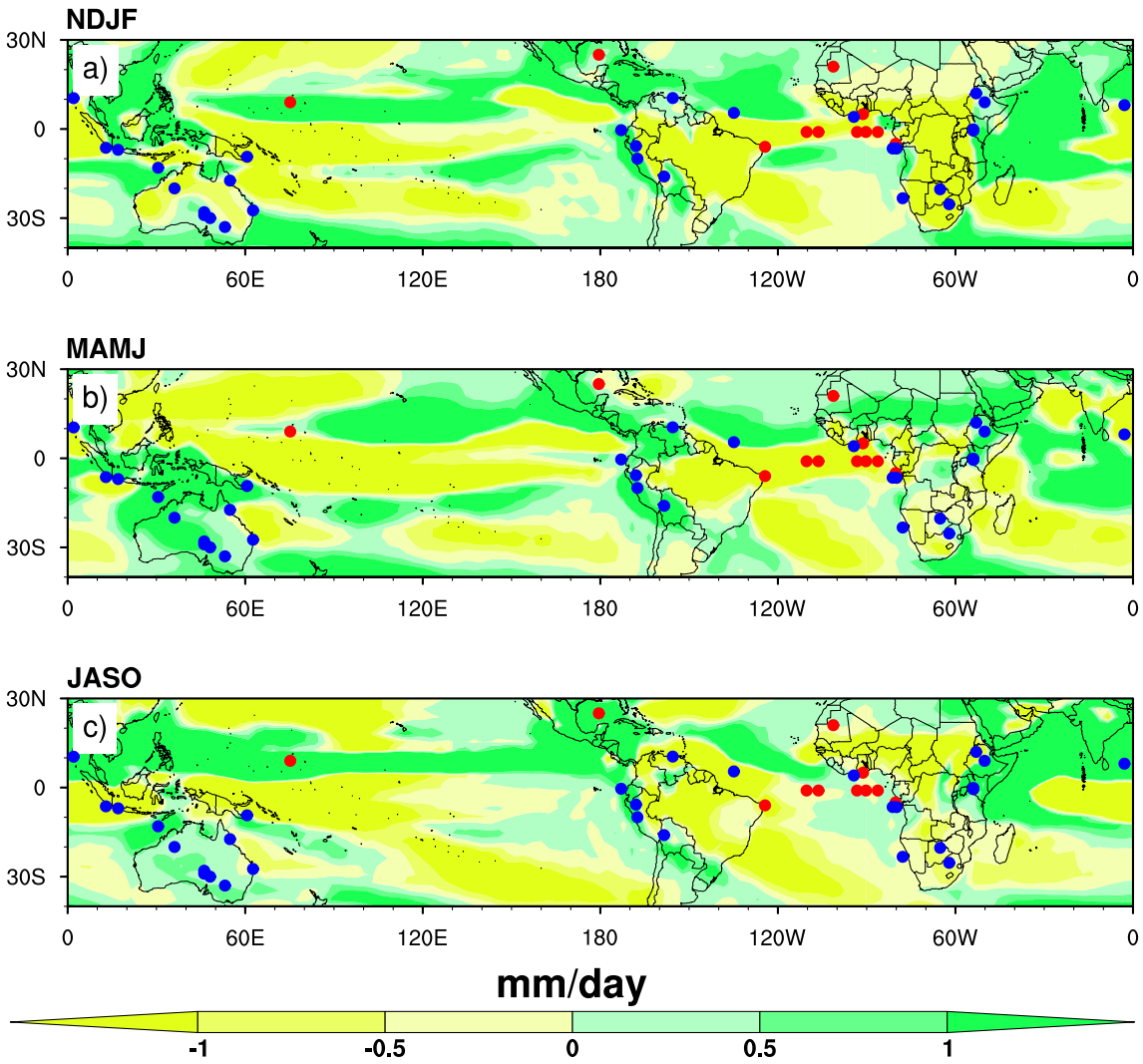

Fig. 9 Map showing precipitation differences between MIS5e and CRTL simulations overlaid by proxy records (wet-blue dots and dry-red dots) during the MIS5e, with respect the present day; for NDJF (**a**), MAMJ (**b**) and JASO (**c**)

Table 4 Maximum values of SST records and modeling results for each interglacial

Site	Coordinates	MIS5e	MIS11c	MIS31	References
		R Δ_{SST}	R Δ_{SST}	R Δ_{SST}	
Lake E	67° N–172° E	14.5 [− 0.32]	12.2 [1.3]	14.3 [− 1.8]	Melles et al. (2012)
ODP 982	57° N–15° W	16.2 [0.71]	15.0 [1.49]	13.8 [− 3.0]	Lawrence et al. (2009)
DSDP 552s	56° N–23° W	15.1 [2.31]	16.4 [0.05]		Ruddiman et al. (1986)
DSDP607	41° N–31° W	29.1 [1.4]		17.5 [− 0.6]	Raymo et al. (1996)
306-U1313	41° N–32° W			18.0 [− 1.1]	Naafs et al. (2013)
ODP 1020	41° N–126° W	14.1 [6.41]	14.0 [6.37]		Herbert et al. (2001)
DSDP 607s	56° N–32° W	25.1 [− 0.53]	26.8 [− 3.42]		Ruddiman et al. (1989)
ODP 1012	32° N–118° W	19.5 [− 0.05]	19.1 [5.9]		Liu et al. (2005)
ODP 1146	19° N–116° E	27.3 [3.94]	26.8 [3.73]	26.0 [− 1.0]	Herbert et al. (2010)
ODP 722	16° N–60° E	27.7 [3.51]	27.5 [3.36]	27.0 [1.0]	Herbert et al. (2010)
ODP 1143	9° N–113° E	28.8 [3.14]	28.3 [3.0]	28.3 [− 0.8]	Li et al. (2011)
ODP 871	5° N–172° E			29.3 [− 0.4]	Dyez and Ravelo (2014)
HY04	4° N–95° W	27.2 [1.34]	26.3 [2.19]		Horikawa et al. (2010)
MD97-2140	2° N–141° E	29.5 [0.14]	29.5 [0.58]		de Garidel-Thoron et al. (2005)
ODP 806B	0.3° N–159° E	29.6 [1.03]	30.2 [− 0.08]		Medina-Elizalde and Lea (2005)
ODP 847	0–95° W			25.6 [− 0.6]	Medina-Elizalde et al. (2008)
ODP 849	0–110° W			25.8 [− 0.8]	McClymont and Rosell-Melé (2005)
ODP 846	3° S–90° W	25.1 [0.69]	24.0 [2.49]	24.3 [0.5]	Herbert et al. (2010)
MD-06-301	23° S–166° E			25.0 [− 1.1]	Russon et al. (2011)
ODP 1087	31° S–15° E			18.0 [− 0.3]	McClymont et al. (2005)
ODP 1123	41° S–171° W	17.7 [− 0.61]	19.3 [− 3.25]	16.0 [0.8]	Crundwell et al. (2008)
ODP 1090	43° S–9° E	17.1 [− 2.16]	13.9 [0.14]	11.5 [− 1.7]	Martínez-Garcia et al. (2010)
MD06-2986	43° S–168° E	18.0 [− 3.12]	18.1 [− 2.51]		Hayward et al. (2012)
DSDP594	45° S–175° E	18.3 [− 4.9]	17.5 [− 5.85]		Schaefer et al. (2005)
PS75/034-2	54° S–80° W	10.3 [− 0.03]	8.8 [2.19]		Ho et al. (2012)

R represents values of reconstruction. Δ_{SST} (°C) shows differences between ICTP-CGCM results and R

model results, good agreement between these data is found for the MAMJ and JASO months, indicating that reconstructions primary reproduce enhanced precipitation in Australia, Andes and eastern Africa, from March to October during the MIS5e (Fig. 9b, c). Southward to 16°S most proxies indicate wetter conditions in Australia and southern Africa. In contrast, the simulated climate is characterized across land surfaces in southern Africa by drier conditions (Fig. 9a, c). The MIS5e climate shows that the orbital forcing leads to decreased austral summer precipitation, due to anomalous high pressure center which may explain the simulated drought in Southern Africa (Fig. 8a, c).

The ICTP-CGCM simulation matches nicely the reconstructions over Australia and western South America indicating more humid conditions during the MIS5e with respect to CTRL (Fig. 9). Some conditions persist along the months, such as the weakening of the ITCZ, that is supported by both modelled precipitation and reconstructions. In fact, based on reconstruction this depends on the ocean basin. In the Atlantic, it is very clear the most proxies are characterized by lower precipitation during those interglacials. The paterrn is different across the Pacific, where precipitation increases in the equatorial belt along the South America coast. Little information is available for MIS11c regarding moisture. Proxies from Africa and South America allow us to infer that during MIS11c conditions were wetter than during the current climate. For MIS31 there is scarce information which hampers to derive conclusions from comparison between model outputs in this study. But Justino et al. (2019) argue that the link between the ENSO and the Australian monsoon is weakened with respect to the CTRL characteristics, and indicates that changes in AUSM during the MIS31 are more closely connected to hemispherical features than to the equatorial Pacific.

Table 5 Hydroclimate reconstruction and modeled values for MIS5e, MIS11c and MIS31

Site	Coordinates	MIS5e	MIS11c	MIS31	References
GeoB4411-2	5° N –44° W	Wet			Govin et al. (2014)
Gunung Mulu	4° N–114° E	Dry			Carolin et al. (2016)
KS 84067	4° N–4° W	Wet			Frédoux (1994)
MD03-2707	2° N–9° E	Dry			Weldeab et al. (2007)
TR163-19	2° N–90° W	Dry			Lea et al. (2000)
TR163-22	0.5° N–92° W	Dry			Lea et al. (2006)
Lake Magadi	0.1° S–36° E	Wet			Owen et al. (2018)
MD01-3340	0.3° S–128° E	Dry			Dang et al. (2015)
ODP 1239	0.4° S–82° W	Wet	Wet		Rincón-Martínez et al. (2010)
Lake Naivasha	0.5° S–36° E	Wet			Trauth et al. (2001)
M16772	1° S–11° W	Dry			Abrantes (2003)
Lake Challa	3° S–37° E	Dry			Moernaut et al. (2010)
ODP 1077	5° S–10° E	Dry			Uliana et al. (2002)
Cueva del Diamante	5° S–77° W	Wet			Cheng et al. (2013)
SO139-74KL	6° S–103° E	Dry			Lückge et al. (2009)
MD98-2152	6° S–104° E	Wet			Windler et al. (2019)
GeoB1401-4	6° S–9° E	Wet			Gingele et al. (1998)
GeoB1008-3	6° S–10° E	Wet			Govin et al. (2014)
DPDR-I, DPDR-II	7° S–108° E	Wet			Van der Kaars and Dam (1995)
MD05-2925	9° S–151° E	Wet			Lo et al. (2017)
ODP 1229	10° S–77° W	Wet			Contreras et al. (2010)
GLAD7-MAL05-1	11° S–34° E	Dry	Wet		Ivory et al. (2016)
MD01-2378	13° S–121° E	Wet			Kawamura et al. (2006)
Altiplano	16° S–68°W	Wet			Placzek et al. (2013)
Lake Titicaca, LT01-2B	16° S–70° W	Dry			Gosling et al. (2008)
Lynch's Crater	17° S–145° E	Wet			Moss and Kershaw (2007)
MD96-2094	19° S–9° E	Dry			Stuut et al. (2002)
Gregory (Mulan)	20° S–127° E	Wet			Bowler et al. (2001)
Salar de Uyuni	20° S–67° W	Dry			Fritz et al. (2004)
Kalahari - Makgadikgadi	20° S–25° E	Wet			Burrough et al. (2009)
M125-55-7/8	20° S–38° W	Dry			Hou et al. (2020)
Coastal Cordillera	21° S–70° W	Dry			Ritter et al. (2019)
GeoB3911-1	21° S–36° E	Dry			Dupont and Kuhlmann (2017)
MD00-2361	22° S–113° E	Dry			Stuut et al. (2014)
MD08-3167	23° S–12° E	Wet			Collins et al. (2014)
Pretoria Saltpan	25° S–28° E	Wet			Partridge et al. (1997)
MD96-2098	25° S–13° E	Dry			Daniau et al. (2013)
MD96-2048	26° S–34° E	Dry			Caley et al. (2018)
Frern Gully Lagoon	27° S–153° E	Wet			Kemp et al. (2020)
Lake Eyre	28° S–137° E	Wet			Magee et al. (2004)
ODP1085	29° S–13° E		Wet		Dickson et al. (2010)
KT-LE	29° S–137° E	Wet			Miller et al. (2016)
Frome	30° S–139° E	Wet			Miller et al. (2016)
CD154-10-06P	31° S–9° E	Dry			Simon et al. (2015)
PA	32° S–137° E	Dry			Miller et al. (2016)
Darling	33° S–144° E	Wet			Miller et al. (2016)

Values indicate wet or dry conditions in reconstructions

4 Concluding remarks

Limitation about our conclusions arises because results are based on single time-slice simulation which may reproduce the interglacial climates characteristics of the summer peak. It is well known that this approach does not capture the temporal variability of those interglacials in response to slow changes of the orbital forcing. For the time being, these caveats related to our technological capacity that does not support in a suitable time millennial scales climate implementations, the experiments are, however, very useful to investigate seasonal peak conditions allowing to understand how the climate system is affected by strengthened radiative forcing, leading to NH warming and/or SH cooling.

This study indicates that the Austral summer monsoons were severely affected during the MIS5e, MIS11c and the MIS31 interglacials due to changes in orbital insolation, which further modifies the SSTs and global teleconnection patterns. Indeed, changes in the precessional cycle triggered significant cooling across Southern Oceans. In the SAMS region, for example, MIS5e and MIS11c show a decrease in the transport of moisture from the Amazon to southeastern South America. The contribution of continental dry air mass favored the decrease of summer monsoon rainfall, and the lower SST during these interglacials, leads to a northward displacement of the SASM, as well as of the SACZ.

Changes of precipitation in summer for the MIS5e and MIS11c stages are dominated by enhanced rainfall in the SH winter and early spring for SAFM, and winter/autumm for AUSM. Reduced precipitation is related to colder conditions during the SH summer, in particular over the continents. Correlation analyses indicate that large-scale processes, such as ENSO are weaker when compared to control run, in exception of increased significant correlation values over the SAMS. Although ICTP-CGCM performs well in reproducing the current climate, the lack of paleoreconstruction data makes it difficult to analyze interglacial periods prior to MIS5e.

Comparison between palaeoreconstructions and model simulations also revealed a good agreement for the analyzed interglacials. It is worth noting that the palaeoproxies deliver the main response to a particular forcing, but does not indicate the preferential season of occurrence. The use of paleo-proxies is always subject of uncertainties because it reproduces local conditions, where climate models deliver values based on areal averages. In addition, results do not show transient climate as may be reproduced by proxies. However, the current study provided an attempt to compare the modeled interglacial climates with paleoreconstruction, but discrepancies can unfortunately be found, because those intervals, which occurred under very particular conditions and high seasonality, may have been dominated by vegetation patterns different than today, modifying the global evaporation rates and the hydrological cycle.

Climate simulations aiming at reproducing the monsoonal system have indicated that enhanced Northern Hemisphere warming can modify the temporal and spatial pattern of Southern Hemisphere precipitation. In a palaeoclimate perspective, this may be similar to conditions during Dansgaard-Oeschger events by means of the two hemispheres seesaw Stocker and Johnsen (2003). To some extent, recent global warming (GW) also shows warmer Boreal climate as delivered by interglacials stages. Therefore, future GW may also result in modified SH monsoonal precipitation with potential to impact the environment and vulnerable population. The understanding of past events could bring important insight on the expected behavior of the climate system and monsoonal precipitation in the future.

Acknowledgements The authors want to thank the funding support of CAPES to project Research Group on Climate Interaction (InteraC), and CNPq funding 303882/2020. PhD Student Carlos Gurjão and Dr, Flávio Justino designed the study, performed data processing, and plotting, and wrote large portions of the manuscript. Dr. Douglas Lindemann contributed with the model simulations. ERA5 is also acknowledged for providing the reanalysis data set.

Funding This work was funded by Coordenação de Aperfeiçoamento de Pessoal de Nível Superior; Conselho Nacional de Desenvolvimento Científico e Tecnológico (Grant no. 303882/2020).

Data availability Enquiries about data availability should be directed to the authors.

Declarations

Conflict of interest The authors have not disclosed any competing interests

References

Abrantes F (2003) A 340,000 year continental climate record from tropical africa-news from opal phytoliths from the equatorial atlantic. Earth Planet Sci Lett 209(1–2):165–179

Bard E, Hamelin B, Fairbanks RG (1990) U-th ages obtained by mass spectrometry in corals from barbados: sea level during the past 130,000 years. Nature 346(6283):456–458

Bereiter B, Eggleston S, Schmitt J, Nehrbass-Ahles C, Stocker TF, Fischer H, Kipfstuhl S, Chappellaz J (2015) Revision of the epica dome c co2 record from 800 to 600 kyr before present. Geophys Res Lett 42(2):542–549

Berger A (1978) Long-term variations of daily insolation and quaternary climatic changes. J Atmos Sci 35(12):2362–2367

Berger A, Loutre MF (1991) Insolation values for the climate of the last 10 million years. Quat Sci Rev 10(4):297–317

Bowler JM, Wyrwoll KH, Lu Y (2001) Variations of the northwest australian summer monsoon over the last 300,000 years: the paleohydrological record of the gregory (mulan) lakes system. Quat Int 83:63–80

Braconnot P, Marzin C, Grégoire L, Mosquet E, Marti O (2008) Monsoon response to changes in Earth's orbital parameters: comparisons between simulations of the Eemian and of the Holocene. Clim Past 4(4):281–294

Braconnot P, Harrison S, Kageyama M, Bartlein P, Masson-Delmotte V, Abe-Ouchi A, Otto-Bliesner B, Zhao Y (2012) Evaluation of climate models using palaeoclimate data. Nat Clim Change 2:417–424. https://doi.org/10.1038/NCLIMATE1456

Burrough SL, Thomas DS, Bailey RM (2009) Mega-lake in the kalahari: a late pleistocene record of the palaeolake makgadikgadi system. Quat Sci Rev 28(15–16):1392–1411

Cabos W, de la Vara A, Koseki S (2019) Tropical atlantic variability: observations and modeling. Atmosphere 10(9) https://www.mdpi.com/2073-4433/10/9/502

Caley T, Extier T, Collins JA, Schefuß E, Dupont L, Malaizé B, Rossignol L, Souron A, McClymont EL, Jimenez-Espejo FJ et al (2018) A two-million-year-long hydroclimatic context for hominin evolution in southeastern africa. Nature 560(7716):76–79

Carolin SA, Cobb KM, Lynch-Stieglitz J, Moerman JW, Partin JW, Lejau S, Malang J, Clark B, Tuen AA, Adkins JF (2016) Northern borneo stalagmite records reveal west pacific hydroclimate across mis 5 and 6. Earth Planet Sci Lett 439:182–193

Carré M, Braconnot P, Elliot M, D'agostino R, Schurer A, Shi X, Marti O, Lohmann G, Jungclaus J, Cheddadi R et al (2021) High-resolution marine data and transient simulations support orbital forcing of enso amplitude since the mid-holocene. Quat Sci Rev 268:107125

Cheng H, Sinha A, Cruz FW, Wang X, Edwards RL, d'Horta FM, Ribas CC, Vuille M, Stott LD, Auler AS (2013) Climate change patterns in amazonia and biodiversity. Nat Commun 4(1):1–6

Clement AC, Cane MA, Seager R (2001) An orbitally driven tropical source for abrupt climate change. J Clim 14(11):2369–2375

Coletti A, DeConto R, Brigham-Grette J, Melles M (2015) A gcm comparison of pleistocene super-interglacial periods in relation to lake el'gygytgyn, ne arctic russia. Clim Past 11(7):979–989

Collini EA, Berbery EH, Barros VR, Pyle ME (2008) How does soil moisture influence the early stages of the south american monsoon? J Clim 21(2):195–213. https://doi.org/10.1175/2007JCLI1846.1

Collins JA, Schefuß E, Govin A, Mulitza S, Tiedemann R (2014) Insolation and glacial-interglacial control on southwestern african hydroclimate over the past 140 000 years. Earth Planet Sci Lett 398:1–10

Contreras S, Lange CB, Pantoja S, Lavik G, Rincón-Martínez D, Kuypers MM (2010) A rainy northern atacama desert during the last interglacial. Geophys Res Lett 37(23)

Crundwell M, Scott G, Naish T, Carter L (2008) Glacial-interglacial ocean climate variability from planktonic foraminifera during the mid-pleistocene transition in the temperate southwest pacific, odp site 1123. Palaeogeogr Palaeoclimatol Palaeoecol 260(1–2):202–229

D'Agostino R, Brown JR, Moise AF, Nguyen H, Dias PLS, Jungclaus JH (2020) Contrasting southern hemisphere monsoon response: mid-holocene orbital forcing versus future greenhouse gas-induced global warming. J Clim 33:9595–9613. https://doi.org/10.1175/JCLI-D-19-0672.1

Dang H, Jian Z, Kissel C, Bassinot F (2015) Precessional changes in the western equatorial p acific hydroclimate: A 240 kyr marine record from the h almahera s ea, e ast i ndonesia. Geochem Geophys Geosyst 16(1):148–164

Daniau AL, Goñi MFS, Martinez P, Urrego DH, Bout-Roumazeilles V, Desprat S, Marlon JR (2013) Orbital-scale climate forcing of grassland burning in southern africa. Proc Natl Acad Sci 110(13):5069–5073

de Garidel-Thoron T, Rosenthal Y, Bassinot F, Beaufort L (2005) Stable sea surface temperatures in the western pacific warm pool over the past 1.75 million years. Nature 433(7023):294–298

Dickson AJ, Leng MJ, Maslin MA, Röhl U (2010) Oceanic, atmospheric and ice-sheet forcing of south east atlantic ocean productivity and south african monsoon intensity during mis-12 to 10. Quat Sci Rev 29(27–28):3936–3947

Dupont LM, Kuhlmann H (2017) Glacial-interglacial vegetation change in the zambezi catchment. Quat Sci Rev 155:127–135

Dyez KA, Ravelo AC (2014) Dynamical changes in the tropical pacific warm pool and zonal sst gradient during the pleistocene. Geophys Res Lett 41(21):7626–7633

Flato G, Marotzke J, Abiodun B, Braconnot P, Chou SC, Collins W, Cox P, Driouech F, Emori S, Eyring V et al (2014) Evaluation of climate models. In: Climate change 2013: the physical science basis. Contribution of working group I to the fifth assessment report of the intergovernmental panel on climate change. Cambridge University Press, pp 741–866

Foley JA (1995) Numerical models of the terrestrial biosphere. J Biogeogr 837–842

Frédoux A (1994) Pollen analysis of a deep-sea core in the gulf of guinea: vegetation and climatic changes during the last 225,000 years bp. Palaeogeogr Palaeoclimatol Palaeoecol 109(2–4):317–330

Fritz SC, Baker PA, Lowenstein TK, Seltzer GO, Rigsby CA, Dwyer GS, Tapia PM, Arnold KK, Ku TL, Luo S (2004) Hydrologic variation during the last 170,000 years in the southern hemisphere tropics of south america. Quat Res 61(1):95–104

Geen R, Bordoni S, Battisti DS, Hui K (2020) Monsoons, ITCZs, and the concept of the global monsoon. Rev Geophys 58(4):e2020RG000700

Gingele F, Müller P, Schneider R (1998) Orbital forcing of freshwater input in the zaire fan area-clay mineral evidence from the last 200 kyr. Palaeogeogr Palaeoclimatol Palaeoecol 138(1–4):17–26

Gosling WD, Bush MB, Hanselman JA, Chepstow-Lusty A (2008) Glacial-interglacial changes in moisture balance and the impact on vegetation in the southern hemisphere tropical andes (bolivia/peru). Palaeogeogr Palaeoclimatol Palaeoecol 259(1):35–50

Govin A, Chiessi CM, Zabel M, Sawakuchi A, Heslop D, Hörner T, Zhang Y, Mulitza S (2014) Terrigenous input off northern south america driven by changes in amazonian climate and the north brazil current retroflection during the last 250 ka. Clim Past 10(2):843–862

Hayward BW, Sabaa AT, Kolodziej A, Crundwell MP, Steph S, Scott GH, Neil HL, Bostock HC, Carter L, Grenfell HR (2012) Planktic foraminifera-based sea-surface temperature record in the tasman sea and history of the subtropical front around new zealand, over the last one million years. Mar Micropaleontol 82:13–27

Held IM, Soden BJ (2006) Robust responses of the hydrological cycle to global warming. J Clim 19(21):5686–5699. https://doi.org/10.1175/JCLI3990.1

Herbert T, Schuffert J, Andreasen D, Heusser L, Lyle M, Mix A, Ravelo A, Stott L, Herguera J (2001) Collapse of the california current during glacial maxima linked to climate change on land. Science 293(5527):71–76

Herbert TD, Peterson LC, Lawrence KT, Liu Z (2010) Tropical ocean temperatures over the past 3.5 million years. Science 328(5985):1530–1534

Hersbach H (2016) The era5 atmospheric reanalysis. AGUFM 2016:NG33D-01

Ho SL, Mollenhauer G, Lamy F, Martínez-Garcia A, Mohtadi M, Gersonde R, Hebbeln D, Nunez-Ricardo S, Rosell-Melé A, Tiedemann R (2012) Sea surface temperature variability in the pacific sector of the southern ocean over the past 700 kyr. Paleoceanography 27(4)

Horikawa K, Murayama M, Minagawa M, Kato Y, Sagawa T (2010) Latitudinal and downcore (0–750 ka) changes in nalkane chain lengths in the eastern equatorial pacific. Quat Res 73(3):573–582

Hou A, Bahr A, Schmidt S, Strebl C, Albuquerque AL, Chiessi CM, Friedrich O (2020) Forcing of western tropical south atlantic sea surface temperature across three glacial-interglacial cycles. Global Planet Change 188:103150

Ivory SJ, Blome MW, King JW, McGlue MM, Cole JE, Cohen AS (2016) Environmental change explains cichlid adaptive radiation at lake malawi over the past 1.2 million years. Proc Natl Acad Sci 113(42):11895–11900

Jorgetti T, Silva Dias P, Freitas E (2014) The relationship between south atlantic sst and sacz intensity and positioning. Clim Dyn 42:3077–3086. https://doi.org/10.1007/s00382-013-1998-z

Justino F, Lindemann D, Kucharski F, Wilson A, Bromwich D, Stordal F (2017) Oceanic response to changes in the WAIS and astronomical forcing during the MIS31 superinterglacial. Clim Past 13(9):1081–1095

Justino F, Kucharski F, Lindemann D, Wilson A, Stordal F (2019) A modified seasonal cycle during MIS31 super-interglacial favors stronger interannual ENSO and monsoon variability. Clim Past 15(2):735–749

Justino F, Gurjão C, Lindemann D (2021) Climate response to drastically modified PDO, PNA and NAM in the superinterglacial MIS 31. Boreas. https://doi.org/10.1111/bor.12556

Kawamura H, Holbourn A, Kuhnt W (2006) Climate variability and land-ocean interactions in the indo pacific warm pool: a 460-ka palynological and organic geochemical record from the timor sea. Mar Micropaleontol 59(1):1–14

Kemp C, Tibby J, Arnold L, Barr C, Gadd P, Marshall J, McGregor G, Jacobsen G (2020) Climates of the last three interglacials in subtropical eastern australia inferred from wetland sediment geochemistry. Palaeogeogr Palaeoclimatol Palaeoecol 538:109463

Kucharski F, Molteni F, Bracco A (2006) Decadal interactions between the western tropical pacific and the north atlantic oscillation. Clim Dyn 26(1):79–91

Kucharski F, Ikram F, Molteni F, Farneti R, Kang IS, No HH, King MP, Giuliani G, Mogensen K (2016) Atlantic forcing of pacific decadal variability. Clim Dyn 46(7–8):2337–2351

Lawrence KT, Herbert TD, Brown CM, Raymo ME, Haywood AM (2009) High-amplitude variations in north atlantic sea surface temperature during the early pliocene warm period. Paleoceanography 24(2)

Lea DW, Pak DK, Spero HJ (2000) Climate impact of late quaternary equatorial pacific sea surface temperature variations. Science 289(5485):1719–1724

Lea DW, Pak DK, Belanger CL, Spero HJ, Hall MA, Shackleton NJ (2006) Paleoclimate history of galápagos surface waters over the last 135,000 yr. Quat Sci Rev 25(11–12):1152–1167

Li L, Li Q, Tian J, Wang P, Wang H, Liu Z (2011) A 4-ma record of thermal evolution in the tropical western pacific and its implications on climate change. Earth Planet Sci Lett 309(1–2):10–20

Lisiecki LE, Raymo ME (2005) A pliocene-pleistocene stack of 57 globally distributed benthic δ18o records. Paleoceanography 20(1)

Liu Z, Altabet MA, Herbert TD (2005) Glacial-interglacial modulation of eastern tropical north pacific denitrification over the last 1.8-myr. Geophys Res Lett 32(23)

Liu Z, Zhu J, Rosenthal Y, Zhang X, Otto-Bliesner B, Timmermann A, Smith R, Lohmann G, Zheng W, Timm O (2014) The holocene temperature conundrum. Proc Natl Acad Sci. https://doi.org/10.1073/pnas.1407229111

Lo L, Chang SP, Wei KY, Lee SY, Ou TH, Chen YC, Chuang CK, Mii HS, Burr GS, Chen MT et al (2017) Nonlinear climatic sensitivity to greenhouse gases over past 4 glacial/interglacial cycles. Sci Reports 7(1):1–7

Lückge A, Mohtadi M, Rühlemann C, Scheeder G, Vink A, Reinhardt L, Wiedicke M (2009) Monsoon versus ocean circulation controls on paleoenvironmental conditions off southern sumatra during the past 300,000 years. Paleoceanography 24(1)

Lüthi D, Le Floch M, Bereiter B, Blunier T, Barnola JM, Siegenthaler U, Raynaud D, Jouzel J, Fischer H, Kawamura K et al (2008) High-resolution carbon dioxide concentration record 650,000–800,000 years before present. Nature 453(7193):379

Madec G (2008) Nemo ocean engine. note du pole de modélisation, institut pierre-simon laplace (ipsl). France 27:1288–1619

Madec G (2012) Nemo ocean engine. note du pole de modélisation de l'institut pierre-simon laplace, france, no. 27. issn no. 1288–1619

Madec G, Delecluse P, Imbard M, Lévy C (1998) Opa 8.1 ocean general circulation model reference manual. Note du Pôle de modélisation 11:91p

Magee JW, Miller GH, Spooner NA, Questiaux D (2004) Continuous 150 ky monsoon record from lake eyre, australia: insolation-forcing implications and unexpected holocene failure. Geology 32(10):885–888

Marengo JA, Liebmann B, Grimm AM, Misra V, Silva Dias PL, Cavalcanti IFA, Carvalho LMV, Berbery EH, Ambrizzi T, Vera CS, Saulo AC, Nogues-Paegle J, Zipser E, Seth A, Alves LM (2012) Recent developments on the south american monsoon system. Int J Climatol 32(1):1–21. https://doi.org/10.1002/joc.2254

Martínez-Garcia A, Rosell-Melé A, McClymont EL, Gersonde R, Haug GH (2010) Subpolar link to the emergence of the modern equatorial pacific cold tongue. Science 328(5985):1550–1553

McClymont EL, Rosell-Melé A (2005) Links between the onset of modern walker circulation and the mid-pleistocene climate transition. Geology 33(5):389–392

McClymont EL, Rosell-Melé A, Giraudeau J, Pierre C, Lloyd JM (2005) Alkenone and coccolith records of the mid-pleistocene in the south-east atlantic: Implications for the u37k' index and south african climate. Quat Sci Rev 24(14–15):1559–1572

Medina-Elizalde M, Lea DW (2005) The mid-pleistocene transition in the tropical pacific. Science 310(5750):1009–1012

Medina-Elizalde M, Lea DW, Fantle MS (2008) Implications of seawater mg/ca variability for plio-pleistocene tropical climate reconstruction. Earth Planet Sci Lett 269(3–4):585–595

Melles M, Brigham-Grette J, Minyuk PS, Nowaczyk NR, Wennrich V, DeConto RM, Anderson PM, Andreev AA, Coletti A, Cook TL et al (2012) 2.8 million years of arctic climate change from lake el'gygytgyn, ne russia. Science 337(6092):315–320

Miller GH, Fogel ML, Magee JW, Gagan MK (2016) Disentangling the impacts of climate and human colonization on the flora and fauna of the australian arid zone over the past 100 ka using stable isotopes in avian eggshell. Quat Sci Rev 151:27–57

Moernaut J, Verschuren D, Charlet F, Kristen I, Fagot M, De Batist M (2010) The seismic-stratigraphic record of lake-level fluctuations in lake challa: hydrological stability and change in equatorial east africa over the last 140 kyr. Earth Planet Sci Lett 290(1–2):214–223

Molteni F (2003) Atmospheric simulations using a GCM with simplified physical parametrizations. I: model climatology and variability in multi-decadal experiments. Clim Dyn. https://doi.org/10.1007/s00382-002-0268-2

Montoya M, von Storch H, Crowley TJ (2000) Climate simulation for 125 kyr bp with a coupled ocean-atmosphere general circulation model. J Clim 13(6):1057–1072

Moss PT, Kershaw AP (2007) A late quaternary marine palynological record (oxygen isotope stages 1 to 7) for the humid tropics of northeastern australia based on odp site 820. Palaeogeogr Palaeoclimatol Palaeoecol 251(1):4–22

Naafs BDA, Hefter J, Gruetzner J, Stein R (2013) Warming of surface waters in the mid-latitude north atlantic during heinrich events. Paleoceanography 28(1):153–163

Neelin JD, Latif M, Jin F (1994) Dynamics of coupled ocean-atmosphere models: the tropical problem. Ann Rev Fluid Mech 26(1):617–659. https://doi.org/10.1146/annurev.fl.26.010194.003153

Nogués-Paegle J, Mechoso CR, Fu R, Berbery EH, Chao WC, Chen TC, Cook K, Diaz AF, Enfield D, Ferreira R et al (2002) Progress in pan american clivar research: understanding the south american monsoon. Meteorologica 27(12):1–30

Oppo D, McManus J, Cullen J (1998) Abrupt climate events 500,000 to 340,000 years ago: evidence from subpolar north atlantic sediments. Science 279(5355):1335–1338

Otto-Bliesner BL, Brady EC, Zhao A, Brierley CM, Axford Y, Capron E, Govin A, Hoffman JS, Isaacs E, Kageyama M et al (2021) Large-scale features of last interglacial climate: results from evaluating the lig127k simulations for the coupled model intercomparison project (cmip6)-paleoclimate modeling intercomparison project (pmip4). Clim Past 17(1):63–94

Owen RB, Muiruri VM, Lowenstein TK, Renaut RW, Rabideaux N, Luo S, Deino AL, Sier MJ, Dupont-Nivet G, McNulty EP et al (2018) Progressive aridification in east africa over the last half million years and implications for human evolution. Proc Natl Acad Sci 115(44):11174–11179

Partridge T, Demenocal P, Lorentz S, Paiker M, Vogel J (1997) Orbital forcing of climate over south africa: a 200,000-year rainfall record from the pretoria saltpan. Quat Sci Rev 16(10):1125–1133

Peltier W, Solheim L (2004) The climate of the earth at last glacial maximum: statistical equilibrium state and a mode of internal variability. Quat Sci Rev 23(3–4):335–357

Pezzi L, Quadro M, Lorenzzetti J, Miller A, Rosa E, Lima L, Sutil U (2022) The effect of oceanic south atlantic convergence zone episodes on regional sst anomalies: the roles of heat fluxes and upper-ocean dynamics. Clim Dyn. https://doi.org/10.1007/s00382-022-06195-3

Placzek C, Quade J, Patchett P (2013) A 130 ka reconstruction of rainfall on the bolivian altiplano. Earth Planet Sci Lett 363:97–108

Raymo M, Grant B, Horowitz M, Rau G (1996) Mid-pliocene warmth: stronger greenhouse and stronger conveyor. Mar Micropaleontol 27(1–4):313–326

Rincón-Martínez D, Lamy F, Contreras S, Leduc G, Bard E, Saukel C, Blanz T, Mackensen A, Tiedemann R (2010) More humid interglacials in ecuador during the past 500 kyr linked to latitudinal shifts of the equatorial front and the intertropical convergence zone in the eastern tropical pacific. Paleoceanography 25(2)

Ritter B, Wennrich V, Medialdea A, Brill D, King G, Schneiderwind S, Niemann K, Fernández-Galego E, Diederich J, Rolf C et al (2019) Climatic fluctuations in the hyperarid core of the atacama desert during the past 215 ka. Sci Reports 9(1):1–13

Rousseau DD, Puisségur JJ, Lécolle F (1992) West-european terrestrial molluscs assemblages of isotopic stage 11 (middle pleistocene): climatic implications. Palaeogeogr Palaeoclimatol Palaeoecol 92(1–2):15–29

Ruddiman W, Shackleton N, McIntyre A (1986) North atlantic sea-surface temperatures for the last 1.1 million years. Geol Soc Lond Special Publ 21(1):155–173

Ruddiman WF, Raymo M, Martinson D, Clement B, Backman J (1989) Pleistocene evolution: Northern hemisphere ice sheets and north atlantic ocean. Paleoceanography 4(4):353–412

Russon T, Elliot M, Sadekov A, Cabioch G, Corrège T, De Deckker P (2011) The mid-pleistocene transition in the subtropical southwest pacific. Paleoceanography 26(1)

Satoh M, Stevens B, Judt F, Khairoutdinov M, Lin SJ, Putman WM, Düben P (2019) Global cloud-resolving models. Curr Clim Change Reports 5(3):172–184

Schaefer G, Rodger JS, Hayward BW, Kennett JP, Sabaa AT, Scott GH (2005) Planktic foraminiferal and sea surface temperature record during the last 1 myr across the subtropical front, southwest pacific. Mar Micropaleontol 54(3–4):191–212

Sicha M, Biton E, Gildor H (2015) Red sea circulation during marine isotope stage 5e. Paleoceanography 30(4):384–401

Simon MH, Ziegler M, Bosmans J, Barker S, Reason CJ, Hall IR (2015) Eastern south african hydroclimate over the past 270,000 years. Sci Reports 5(1):1–10

Stocker TF, Johnsen SJ (2003) A minimum thermodynamic model for the bipolar seesaw. Paleoceanography 18(4):1087. https://doi.org/10.1029/2003PA000920

Stuut JBW, Prins MA, Schneider RR, Weltje GJ, Jansen JF, Postma G (2002) A 300-kyr record of aridity and wind strength in southwestern africa: inferences from grain-size distributions of sediments on walvis ridge, se atlantic. Mar Geol 180(1–4):221–233

Stuut JBW, Temmesfeld F, De Deckker P (2014) A 550 ka record of aeolian activity near north west cape, australia: inferences from grain-size distributions and bulk chemistry of se indian ocean deep-sea sediments. Quat Sci Rev 83:83–94

Timm O, Timmermann A, Abe-Ouchi A, Saito F, Segawa T (2008) On the definition of seasons in paleoclimate simulations with orbital forcing. Paleoceanography. https://doi.org/10.1029/2007PA001461

Timmermann A, Lorenz S, An S, Clement A, Xie S (2007) The effect of orbital forcing on the mean climate and variability of the tropical pacific. J Clim 20(16):4147–4159

Tomita H, Miura H, Iga SI, Nasuno T, Satoh M (2005) A global cloud-resolving simulation: preliminary results from an aqua planet experiment. Geophys Res Lett 32(8)

Trauth MH, Deino A, Strecker MR (2001) Response of the east african climate to orbital forcing during the last interglacial (130–117 ka) and the early last glacial (117–60 ka). Geology 29(6):499–502

Trenberth KE (2011) Changes in precipitation with climate change. Clim Res 47(1–2):123–138

Uliana E, Lange CB, Wefer G (2002) Evidence for congo river freshwater load in late quaternary sediments of odp site 1077 (5 s, 10 e). Palaeogeogr Palaeoclimatol Palaeoecol 187(1–2):137–150

Valcke S (2013) The oasis3 coupler: a european climate modelling community software. Geosci Model Dev 6(2):373–388

Valdes PJ, Scotese CR, Lunt DJ (2021) Deep ocean temperatures through time. Clim Past 17(4):1483–1506

Van der Kaars W, Dam M (1995) A 135,000-year record of vegetational and climatic change from the bandung area, west-java, indonesia. Palaeogeogr Palaeoclimatol Palaeoecol 117(1–2):55–72

Weldeab S, Lea DW, Schneider RR, Andersen N (2007) 155,000 years of west african monsoon and ocean thermal evolution. Science 316(5829):1303–1307

Wild M (2020) The global energy balance as represented in cmip6 climate models. Clim Dyn 55:553–577. https://doi.org/10.1007/s00382-020-05282-7

Windler G, Tierney JE, DiNezio PN, Gibson K, Thunell R (2019) Shelf exposure influence on indo-pacific warm pool climate for the last 450,000 years. Earth Planet Sci Lett 516:66–76

Yim SY, Wang B, Liu J, Wu Z (2014) A comparison of regional monsoon variability using monsoon indices. Clim Dyn 43(5–6):1423–1437

Yin Q, Berger A (2012) Individual contribution of insolation and CO2 to the interglacial climates of the past 800,000 years. Clim Dyn 38:709–724. https://doi.org/10.1007/s00382-011-1013-5

Zhao X, Cheng H, Sinha A, Zhang H, Baker JL, Chen S, Kong X, Wang Y, Edwards RL, Ning Y et al (2019) A high-resolution speleothem record of marine isotope stage 11 as a natural analog to holocene asian summer monsoon variations. Geophys Res Lett 46(16):9949–9957